Energy & Environmental Science

Direct Conversion of Thermal Energy to Stored Electrochemical Energy via a Self-Charging Pyroelectrochemical Cell

Journal:	*Energy & Environmental Science*
Manuscript ID	EE-ART-10-2023-003497.R1
Article Type:	Paper
Date Submitted by the Author:	05-Jan-2024
Complete List of Authors:	Kowalchik, Tim; The University of Utah, Mechanical Engineering Khan, Fariha; The University of Utah, Electrical Engineering Horlacher, Danielle; The University of Utah, Mechanical Engineering Roundy, Shad; The University of Utah, Mechanical Engineering Warren, Roseanne; University of Utah, Mechanical Engineering

Greater Context

Tim Kowalchik, Fariha Khan, Danielle Horlacher, Shad Roundy, and Roseanne Warren*

Direct Conversion of Thermal Energy to Stored Electrochemical Energy *via* a Self-Charging Pyroelectrochemical Cell

This work is focused on a novel form of energy generation we term the Pyroelectrochemical Cell (PEC), a type of self-charging supercapacitor. In the world of Internet of Things (IoT) and wireless sensing, the power sources available for use are one of the greatest limiting factor for practical applications. The PEC is capable of charging when exposed to a thermal input, gathering and storing energy in a single device at levels suitable for low-power wireless sensing tasks. The self-charging cell replaces more toxic energy sources like batteries, reducing the environmental impact of IoT systems. This work focuses on experimental and simulated results validating the fundamental physics of the PEC, confirming its energy production and identifying possible routes for future improvement and use.

Direct Conversion of Thermal Energy to Stored Electrochemical Energy *via* a Self-Charging Pyroelectrochemical Cell

*Tim Kowalchik, Fariha Khan, Danielle Horlacher, Shad Roundy, and Roseanne Warren**

T. Kowalchik, D. Horlacher, S. Roundy, R. Warren

Department of Mechanical Engineering, University of Utah

1495 E 100 S, 1550 MEK

Salt Lake City, Utah 84112, USA

*Email: roseanne.warren@utah.edu

F. Khan

Department of Electrical and Computer Engineering, University of Utah

50 S. Central Campus Drive, MEB Room 2110

Salt Lake City, Utah 84112, USA

*Corresponding Author

Keywords: Pyroelectricity. Supercapacitors. Energy Harvesting. Electrochemistry. Internet-of-Things

Abstract

This work investigates a pyroelectrochemical cell (PEC) as a novel device concept for direct conversion of thermal energy to stored electrochemical energy. The PEC integrates a porous, pyroelectric separator within a supercapacitor. The pyroelectric separator induces an electric field within the PEC when exposed to a temperature change with time. The electric field drives ions into electrode double layers to charge the cell. Experimental results are coupled with simulations to explore PEC response when thermally cycled, with predicted pyroelectric orientation effects observed in two tests. When tested through amperometry, the pyroelectric separator showed a 155% increase in measured current upon heating compared to a 35% increase in measured current for a non-pyroactive separator. Under open circuit conditions, the PEC charged by 0.65 mV after four applications of a 20-30-20 ^{o}C thermal cycle. Finite element simulations confirm that the PEC self-charges by pyroelectric field-driven ion flux. With optimization of the pyroelectric separator, the PEC is predicted to generate >100 μJ/cm^2 of energy from temperature fluctuations commonly found in natural and built environments, making the PEC an exciting new energy source for low power Internet of Things sensors.

1. Introduction

In recent years, the concept of Internet of Things (IoT) has seen growing interest and technological development. IoT systems consist of interconnected sensing devices that provide detailed information about a zone or phenomenon of interest. Application areas implementing IoT systems include smart agriculture, manufacturing, healthcare monitoring, and energy management.[1-4] A central challenge to IoT implementation is powering an array of sensors in a self-sustaining manner with low spatial footprint. Traditional energy storage devices, such as batteries, require regular charging to keep the IoT system online, while energy harvesting devices lack storage for on-demand power availability. The development of innovative methods of coupling ambient energy harvesting and energy storage in a small footprint, low volume device, is critical to the development of self-sufficient, real-world IoT systems.

Self-charging power cells are a novel concept for integrating energy harvesting and energy storage functionalities within a single device. In these devices, traditionally inactive components of an electrochemical cell, such as the separator, take on new functionality as energy harvesting materials capable of charging the cell without an external power source. By coupling energy harvesting and storage materials at the cell level, self-charging power cells achieve smaller device footprint, reduced packaging and auxiliary systems, and simpler construction compared to externally-wired systems. Xue *et al.* first introduced the concept of a piezoelectric self-charging supercapacitor powered by under-shoe compressions during walking.[5] This design consisted of a piezoelectric separator placed inside a lithium-ion battery and inserted into the heel of a shoe. The device was capable of storing 0.036 μAh of energy after repeated deformation. The concept has since been expanded to include, *e.g.*: supercapacitors integrated with flexible harvesters charged by hand compression;[6] an all solid-state, piezoelectric self-

charging power cell using solid polymer electrolytes;[7] coupled photovoltaic energy harvesting and storage devices using magnesium oxide-polyvinylidene fluoride (MgO_2-PVDF) composites;[8] and triboelectric-driven self-charging supercapacitors.[9-10]

This work explores a self-charging power cell using pyroelectric energy harvesting that we term a "pyroelectrochemical cell" (PEC) (**Figure 1**). The PEC uses a porous pyroelectric material as the separator of an electrochemical cell, thus integrating thermal energy harvesting with electrochemical energy storage. Low-grade thermal energy is abundant in the environment, yet direct integration of thermal energy harvesting and electrochemical energy storage has only been explored in a limited capacity to-date. Thermogalvanic cells use a spatial temperature gradient between anode and cathode to generate current from temperature-dependent redox reactions.[11] Thermally regenerative electrochemical cycles use a temperature change in time to charge a battery at a lower potential difference than its discharge. The approach requires high-cost ion exchange membranes and is not well-suited to small-scale applications.[12] For IoT systems in environments that experience temperature fluctuations in time, there are currently no technologies for integrating energy harvesting and storage at the device level. The PEC fills this gap by enabling direct conversion of thermal energy–in the form of a change in temperature with time–to stored electrochemical energy for IoT applications. Figure 1a illustrates potential applications of the PEC in, *e.g.*: tire pressure monitoring sensors powered by *dT/dt* at the exhaust pipe of a car, soil sensors powered by diurnal temperature fluctuations, and material health monitoring sensors powered by temperature fluctuations on airplanes or unmanned aerial vehicles (UAVs).

Figure 1 provides a conceptual schematic of the PEC device architecture (Figure 1b) and the theory of operation (Figure 1c). Cell construction is based on a supercapacitor or battery

design, with a porous, pyroelectric film as the separator. Our proposed theory of operation is as follows. By virtue of the pyroelectric effect, the separator in the PEC generates an electric field in response to temperature fluctuations with time. The relevant constitutive equation of pyroelectricity is:

$$dD = \varepsilon^T dE + \boldsymbol{\rho} dT \tag{1}$$

where D is the electrical displacement, ε^T is electric permittivity at constant temperature (simply ε hereafter), E is electric field, $\boldsymbol{\rho}$ is the pyroelectric coefficient, and T is temperature. Assuming the temperature is spatially uniform throughout the pyroelectric material and that the material is in the open circuit condition, Equation 1 reduces to Equation 2:

$$\frac{d\phi}{dx} = -\frac{\boldsymbol{\rho}}{\varepsilon} \cdot \Delta T \tag{2}$$

where ϕ is the electric potential and x is the dimension through the thickness of the separator. This electric field ($E = d\phi/dx$) drives ion migration across the separator, with the resulting ion movement described by the one-dimensional Nernst-Planck equation (Equation 3):

$$\frac{\partial c}{\partial t} = \frac{d}{dx} \cdot \left[D\frac{dc}{dx} - c\boldsymbol{v} + \frac{Dz\mathscr{e}}{k_B T} c\left(\frac{d\phi}{dx} + \frac{\partial \boldsymbol{A}}{\partial t}\right)\right] \tag{3}$$

where c is concentration, D is diffusivity, $\boldsymbol{v}$ is flow velocity, z is ion valence, e is elementary charge, k_B is the Boltzmann constant, and $\boldsymbol{A}$ is the magnetic vector potential. In an electrochemical double layer capacitor (EDLC), this ion flux will result in charged species populating the electric double layers of the cell in response to the pyroelectric field generated upon heating. The charging of the electric double layers will increase the energy stored in the EDLC, U, given by Equation 4:

$$U = \frac{1}{2} C_{dl} V^2 \tag{4}$$

where V is the electric potential across the EDLC (distinct from ϕ which is the potential across the separator) and C_{dl} is the total double layer capacitance (Figure 1c).

In this report we experimentally and computationally validate our theory of PEC charging by examining the electrochemical response of cells subject to controlled heating and cooling cycles. A demonstration PEC is assembled using a porous, electroactive, polyvinylidene fluoride-barium titanate (PVDF-BT) separator and carbon electrodes. The demonstration PEC is a non-Faradaic, electrochemical double-layer type capacitor. Two control cells with non-pyroactive separators (a Celgard 3501 cell and an unpoled PVDF-BT cell) are used to differentiate between thermal and pyroelectric effects occurring within the PEC. Thermal effects are defined as changes in potential or current arising purely from the temperature dependence of electrochemical cell properties including diffusion coefficients, ion mobility, cell capacitance and cell resistance. Two electrochemical measurement approaches are used to probe the PEC response to a thermal input: 1) amperometry, in which the cell is held at a fixed potential and current flow in response to a thermal input is measured; and 2) open circuit potential (OCP), to verify the self-charging nature of the cell in the absence of external current flow. Using these approaches, we investigate the effects of: 1) heating *vs.* cooling, 2) separator polarity (*i.e.* orientation), 3) dT/dt, 4) total temperature change (ΔT) and 5) repeated thermal cycling on the PEC response as suggested by Equations 1-4. A COMSOL Multiphysics® finite element simulation is developed to further investigate PEC device physics. Temperature-dependent cell properties in the simulation are empirically determined through experiments using cyclic voltammetry (CV) and electrochemical impedance spectroscopy (EIS) measurements conducted at fixed temperatures. The effect of a dT/dt input on electric field-driven ion movement is studied in-depth and found to have good agreement with experiment. Finally, we explore potential

improvements in PEC material selection and design to increase device performance and compare predicted cell energy densities with target values for IoT applications for a range of energy harvesting environments.

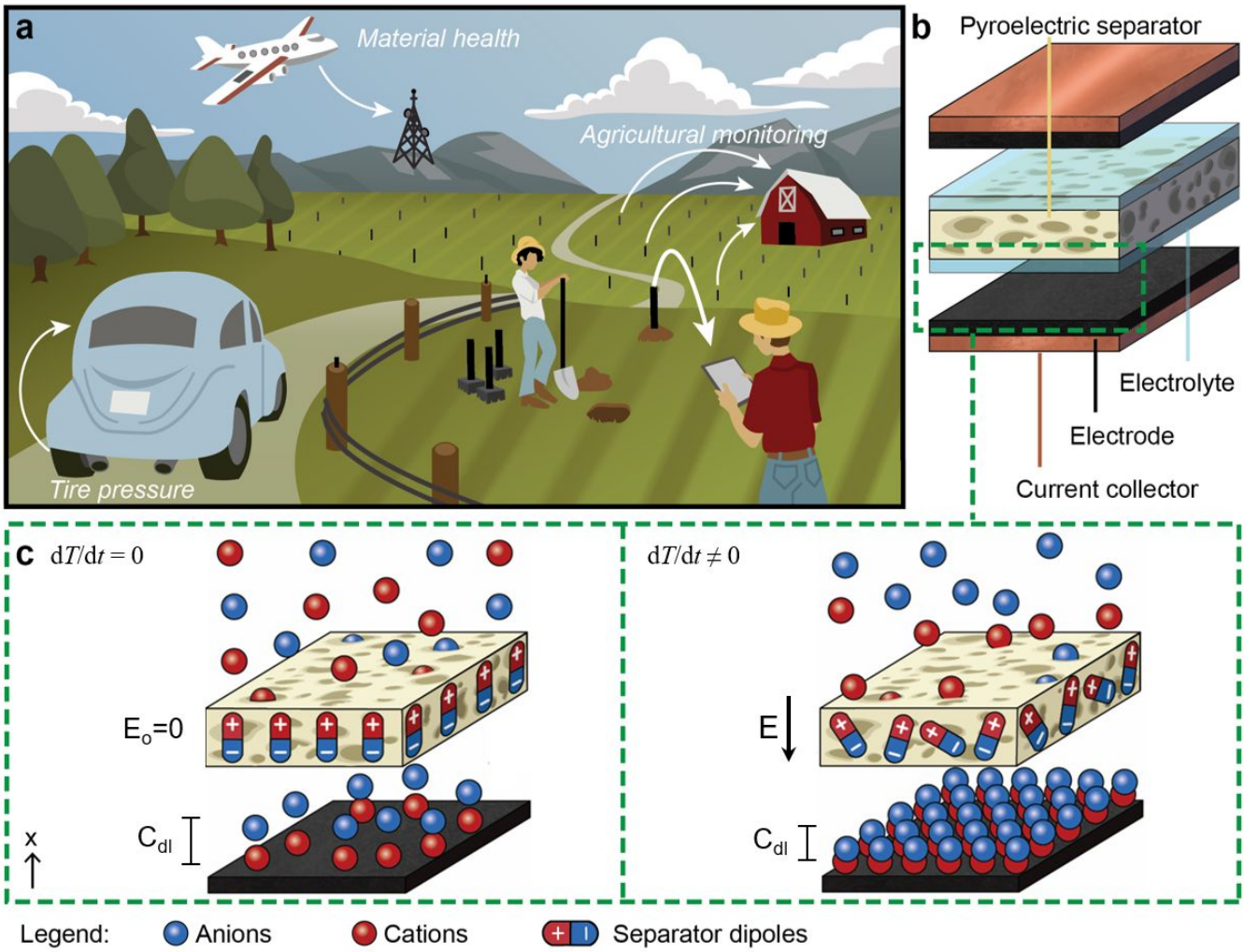

Figure 1. a) Conceptual illustration of PEC-driven wireless IoT sensors. Potential PEC energy sources include soil, vehicle exhaust pipe, and airplane/UAV temperature fluctuations with time. b) PEC device structure including current collectors, electrodes (battery or supercapacitor), electrolyte, and porous pyroelectric separator. c) PEC theory of operation. A PEC at rest will stabilize to some distribution of ions and double layer capacitance C_{dl} in response to the resting cell state and separator field $E_o=0$. Upon heating, the dipoles within the separator become un-aligned, resulting in an induced electric field E within the PEC compared to the rest state. Free ions in the electrolyte react to the field and are driven through the separator, packing the electric double layers of the PEC with more charge and increasing the stored energy.

2. Methods

2.1 PEC Assembly

Porous, pyroelectric PVDF-BT films were fabricated by phase inversion as described in a previous work.[13] Pure DI water was used as the phase inversion bath. Non-pyroelectric PVDF-BT films were fabricated by the same method, without electrostatic poling. The non-pyroelectric films have the same pore structure as the poled, pyroelectric films. Symmetric supercapacitor cells were assembled using graphite on copper electrodes (BR0186, MSE Supplies) (36±0.5 cm^2 per electrode) with 0.5 M Na_2SO_4 electrolyte (Millipore Sigma). Three types of separators were used: 1) electrically poled PVDF-BT, 2) unpoled, non-pyroelectric PVDF-BT, and 3) Celgard 3501 (25 μm microporous monolayer membrane). A custom cell design was used with 3D printed lid, clip and wedge to hold the cell stack together in a sealed glass container (500 ml, Glasslock) (Supporting Information **Figure S1**). A thermocouple (K-type, PerfectPrime) was placed in the cell adjacent to the electrode stack. Cells were sealed with plumbers' putty around the lid and all connections. After construction, cells were allowed to rest for 24 hours before testing.

2.2 PEC Temperature Control

An external water bath was used for cell temperature control during fixed temperature and temperature ramp experiments. The PEC was fully immersed in the water bath during all experiments to minimize in-plane temperature gradients within the cell. Fixed temperature experiments were performed at 20 ^oC and 50 ^oC cell temperatures. A measured cell temperature variation of less than 0.25 ^oC over a period of at least 15 minutes was required before fixed temperature testing began.

Temperature ramp experiments were conducted through the addition and removal of hot or cold water to the bath. Three temperature ramp scenarios were employed: 1) 20-30-20 ^oC, 2)

20-50-20 ^{o}C, and 3) 20-10-20 ^{o}C. Material degradation of 3D printed parts was observed above 60 °C, so a maximum cell temperature of 50 °C was chosen to maintain experimental integrity. Supporting Information **Figure S2** provides measured cell temperature profiles for each ramp scenario. **Table S1** provides water bath temperatures used, and time to reach target temperature. In all subsequent result reporting and discussion, reported temperatures are the cell temperature measured by the internal cell thermocouple.

2.3 PEC Testing

CV, EIS, and amperometry experiments were conducted using a Gamry Reference 600+ potentiostat; OCP experiments were conducted using a Gamry Interface 1000E potentiostat. CV measurements were performed at a scan rate of 100 mV/s over 0–250 mV and 0–400 mV ranges. For all tests conducted sequentially, the cell was discharged through shorting the electrodes for 10 minutes. The cell then rested at room temperature for at least 20 minutes. EIS measurements were conducted over a frequency range of 0.1–100 kHz. Amperometry experiments were conducted at 50 mV and 120 mV constant applied voltage. The voltage was applied at room temperature for 25 minutes before any thermal cycling occurred and held for an additional 10 minutes after the cell returned to room temperature. During OCP experiments, cell OCP was monitored for 24 hours before thermal cycling.

All EIS, CV, and amperometry experiments were conducted at least three times with different cells. OCP experiments were repeated two times. Excellent repeatability was observed between cells and for repeated tests on the same cell, except in the case of the first thermally cycled amperometry experiment, which was excluded from reported results. Supporting Information **Figure S3** provides additional information on repeatability of amperometry experiments.

In testing, two distinct orientations of the pyroelectric separator were used: "anode-facing" and "cathode-facing." In anode-facing orientation, the positive face of the separator is in contact with the cell anode. In cathode-facing orientation, the positive face of the separator is in contact with the cathode. Cathode and anode are defined according to secondary battery convention during charging: the negative electrode is the cathode and the positive electrode is the anode. Pyroelectric separator orientation was reversed in experiments by switching the electrode-potentiostat connections. This method was found to produce fewer uncontrolled changes in the cell *vs*. physically reversing the separator (Supporting Information **Figure S4**).

2.5 PEC Simulation

Finite element simulations of the PEC were conducted in COMSOL Multiphysics®. Two physics branches were used: Electrochemistry (Tertiary Current Distribution) and Heat Transfer (Heat Transfer in Solids and Fluids). A 1-D simulation approximates the cell as four distinct nodes: 1) electrode surface, 2) electrolyte region, 3) separator region, and 4) electrode surface (Supporting Information **Figure S5**). To match the experimental cells, cell length was 150 μm electrode-electrode and the separator thickness was 60 μm. The electrolyte was 0.5 M Na_2SO_4, with temperature-dependent values of ion diffusion coefficient, ion mobility, and permittivity.[14-17] The separator was PVDF with 65% porosity. A custom, graded mesh was set as follows: 1) ultrafine mesh near the electrode surface (> 0.5 nm), 2) course mesh in the electrolyte region (<1 μm), 3) fine mesh near the separator-electrolyte boundary (>0.100 μm), and 4) course mesh within the separator (>0.75 μm) (Supporting Information Figure S5c).

Cell temperature was controlled in the simulation using time-dependent heat inputs replicating experimental temperature curves (Figure S2). The pyroelectric response of the separator was represented as a temperature-dependent voltage. Film pyroelectricity was

measured previously by sputtering gold electrodes onto prepared films and measuring the voltage response when the films were heated.[18] Cell voltage was defined in the model as the potential difference between the electrode surfaces. Current was defined as the total current through the cell. Mechanical stresses, thermal expansion, leakage current, and thermal losses were neglected in the simulation. No external resistance or other losses were considered. The electrolyte was assumed to fully dissociate. Additional details regarding the simulation are provided in the Supporting Information.

3. Results and Discussion

3.1 Constant Temperature Response

Figure 2 provides an overview of the PEC device used in this work. The cell consists of symmetric graphite on copper electrodes (anode and cathode), aqueous electrolyte, and a porous, pyroelectric separator (Figure 2a). The pyroelectric separator is a PVDF-BT composite film with 65% porosity and a thickness of 50-60 μm[13] (Figure 2b). PVDF-BT was chosen for its good pyroelectric response, high chemical resistance, and ease of fabrication as a flexible, porous film. Electrically poled PVDF-BT films used in this work have a measured pyroelectric coefficient of 59 $\mu C/m^2*K$.[18] When heated, both the Celgard films and the unpoled PVDF-BT films employed as control separators show a lack of pyroelectric response (Supporting Information **Table S2**). Figure 2c provides an image of the water bath set-up used for electrochemical measurements at constant temperature and under controlled heating/cooling cycles.

CV and EIS measurements of PEC cells were conducted at constant temperature to: 1) test the separator functionality of porous PVDF-BT films; 2) quantify thermal effects in the absence of pyroelectricity; and 2) establish finite element simulation parameters for PVDF-BT and Celgard 3501 cells. Cells constructed with porous PVDF-BT films show comparable EIS and CV response to Celgard 3501 cells (Supporting Information **Figure S6**). At 20 ^oC, PVDF-BT cells have an average equivalent series resistance (ESR) of 24 Ω, compared to 18 Ω for Celgard 3501 cells. The results indicate that porous PVDF-BT films provide good wettability, ionic conductivity, and electrical insulation in their function as an electrochemical separator.

As no pyroelectric effects are present at constant temperature, changes in CV and EIS response of the PEC at 20 ^oC *vs*. 50 ^oC can be attributed to a "thermal" response of the cell. A small change in ESR is observed with increasing temperature, from an average of 24 Ω at 20 ^oC

to an average of 26 Ω at 50 °C (averages taken across multiple cells; Figure 2d plots one set of measurements per temperature condition). While the ESR of a supercapacitor is well known to decrease with increasing temperature, experimental reports with activated carbon electrodes have demonstrated that this change is most significant at temperatures below 25 °C. Above 25 °C, there is less variation in ESR, including some up-down fluctuations, such that the small change observed here is not unexpected.[19] As PEC cell temperature increases from 20°C to 50°C, the Warburg impedance phase angle decreases below 45°. This represents a change from semi-infinite diffusion to finite-length diffusion.[20] This is due to the increase in diffusion coefficient, decrease in electrolyte viscosity, and increase in ion mobility as the cell temperature increases.[21-23] Average PEC capacitance increases slightly with temperature, from 3.2 mF at 20 °C to 3.8 mF at 50 °C, in agreement with published results[24] (Figure 2e).

COMSOL simulation parameters for poled PVDF-BT, unpoled PVDF-BT, and Celgard 3501 cells were established using resistance and capacitance values obtained from CV and EIS measurements of these cells at 20 °C and 50 °C. Using empirical *R* and *C* parameters, good agreement was obtained between simulated CV and EIS curves and experimental measurements, with <5% difference in the case of CV curves (Figure 2d, e). Based on this comparison, the COMSOL model was deemed to have good predictive capabilities of PEC cell behavior over the temperature and voltage ranges to be examined in variable-temperature simulations of ion flux and pyroelectric cell charging/discharging phenomenon.

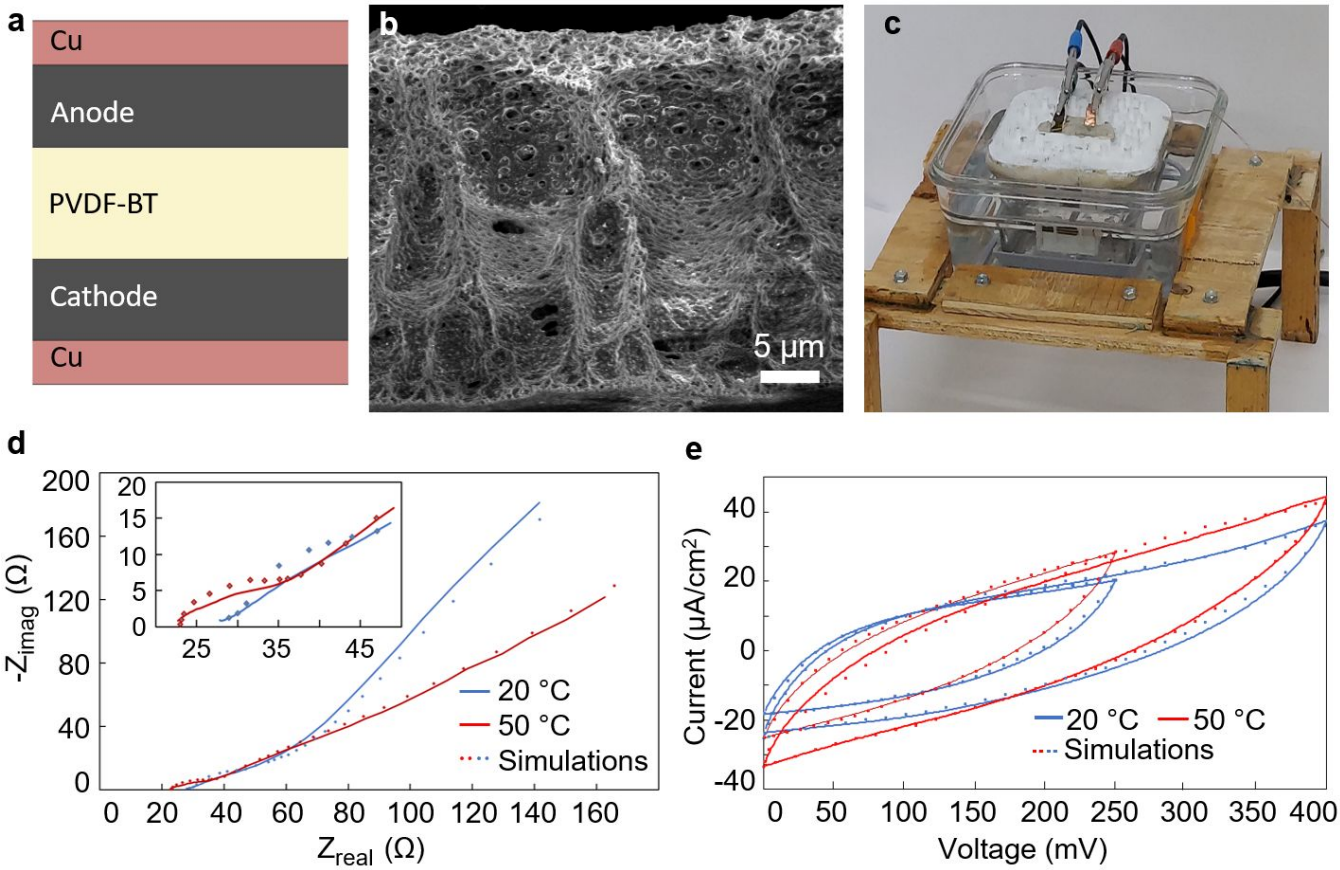

Figure 2. a) Schematic of PEC device of this work, composed of copper current collectors, graphite electrodes, and a pyroelectrically active PVDF-BT separator. b) SEM cross-section of the porous PVDF-BT separator. Reproduced with permission.[13] Copyright 2023, Elsevier. c) PEC test cell immersed in a water bath for temperature-controlled experiments. d) PEC experimental and simulated EIS measurements at cell temperatures of 20 °C and 50 °C. e) PEC experimental and simulated CV measurements at cell temperatures of 20 and 50 °C for 250 mV and 400 mV sweep ranges (PVDF-BT separator used in (d) and (e)).

3.2 Variable Temperature Response: Amperometry

We first explored the response of the PEC to changes in temperature with time (*i.e.*, *dT/dt*) through a series of amperometry tests. Amperometry tests were conducted by applying a constant voltage of 50 mV or 120 mV across the cell and measuring the resulting current through the cell as the temperature was ramped up and down. As illustrated in **Figure 3a**, when a voltage is applied to the cell, cations are driven from anode to cathode by the applied electric field E_a and the resulting current external to the cell, i, is measured. The effective impedance of the electrode, double layer, and electrolyte is temperature dependent, as characterized in the previous section. Thus, even without the pyroelectric separator, the measured current will change with changing temperature. In addition to this basic cell thermal response, the pyroelectric separator will induce an electric field across the separator (shown as E_s in Figure 3a) in response to a change in temperature. If the cell is heating and the separator is in the cathode-facing orientation, this electric field will be in the same direction as the externally applied driving voltage. Thus, the pyroelectric separator will aid the flow of positive ions from anode to cathode relative to the basic cell thermal response. The effect of the pyroelectric separator will be to increase the measured current. If the orientation of the separator is flipped to be anode-facing, we expect the opposite effect, *i.e.*, the pyroelectric separator will impede ion flow. Likewise, if the separator is first cooled rather than heated, we expect E_s to flip direction. We validated the expected PEC behavior by: 1) comparing the thermal response of a cell with a non-PVDF, non-pyroelectric separator (Celgard 3501) to the PEC with the pyroelectric PVDF-BT separator, 2) comparing the thermal response of a cell with an unpoled PVDF-BT (*i.e.*, non-pyroelectric) separator to the response of a PEC with a poled PVDF-BT separator in both anode- and cathode-facing

orientations, and 3) simulating the PEC and observing changes in ion concentration as a result of changing temperature.

We first compared a PEC with an active PVDF-BT separator to a PEC with a commercial Celgard separator (Figure 3b-d). During this amperometric testing, each cell was held at 50 mV, the cells were subject to a 20-30-20 ^{o}C thermal cycle, and the resulting current through the cell was measured. Values are reported as the ratio of current under temperature excitation to the resting state current (designated "Current Ratio (μA/μA)" in Figure 3b-d). The use of a current ratio accounts for the difference in pre-cycling equilibrium current between Celgard and PVDF-BT cells arising from the different separator materials. The Celgard cell showed an increase of 35% comparing the resting current to the current at the maximum temperature of 30 °C. This serves as a measure of the basic thermal response of a supercapacitor of the same construction as the PEC. When a pyroactive PVDF-BT served as the separator, the current increased by 155% from the resting current to the current at 30 °C (Figure 3b). This behavior confirms that the cell with the PVDF-BT separator has a larger response to temperature. In addition to the 20-30-20 °C temperature cycle, we subjected both the Celgard and PVDF-BT cells to a 20-50-20 °C temperature cycle (Figure 3c) and a 20-10-20 °C temperature cycle (Figure 3d). As expected, when the cells are cycled through a higher temperature, the measured current increases in rough proportion to the increase in temperature (*i.e.*, ΔT is tripled and the increase in current ratio is also approximately tripled for both cell types). When the cells are first cooled rather than heated, the measured current drops and then returns to the resting state upon reheating to 20 °C, again following expectations. The measured current ratio for the PVDF-BT cell drops more than for the Celgard cell, indicating an enhanced effect from the pyroelectric separator.

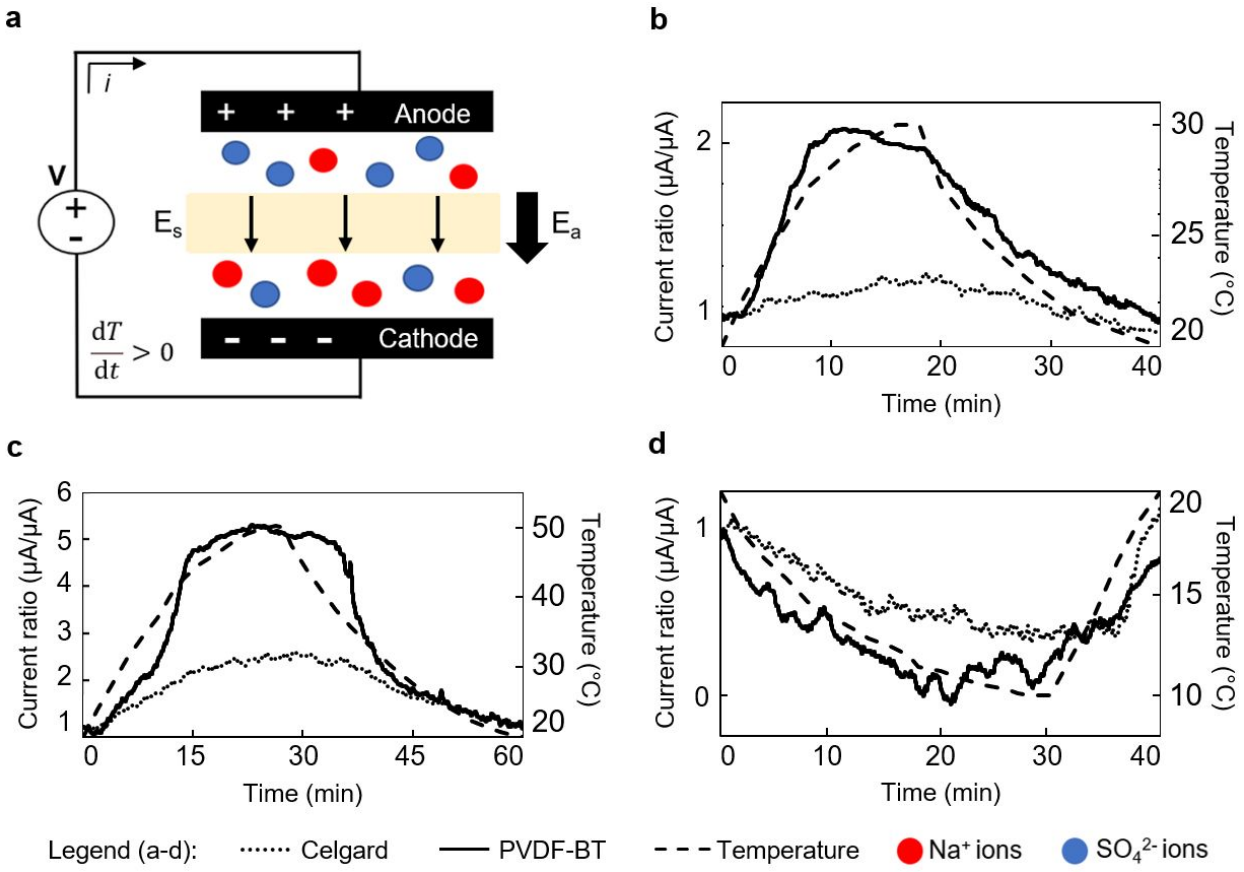

Figure 3. a) Schematic of the proposed PEC function during amperometry. In this 'cathode-facing' orientation, when heated the separator will create an electric field E_s driving negative ions towards the anode and positive ions towards the cathode. b-d) PVDF-BT pyroelectrically active separator *vs.* Celgard cell amperometric testing. Change in amperometric current *vs.* the value at rest for the Celgard and PVDF-BT cells during b) a heating cycle from 20-30-20 °C, c) a heating cycle from 20-50-20 °C, d) and a cooling cycle from 20-10-20 °C.

To further examine the expected PEC behavior with changing temperature, amperometric tests were conducted with the PEC separator in two different orientations: anode-facing and cathode-facing (**Figure 4**). We expect that changing the separator orientation will reverse the effect of the pyroelectric separator. Specifically, during heating with the separator in the cathode-facing orientation (Figure 4a) we expect the separator to drive more positive ions to the cathode and more negative ions to the anode, thus increasing the measured current relative to a cell with a non-pyroelectric separator. Conversely, during heating with the separator in the anode-facing orientation (Figure 4b), we expect the separator to drive more negative ions to the cathode and more positive ions to the anode, thus decreasing the measured current. Referring to Figure 4c-d, during cooling with the separator in the cathode-facing orientation, we expect the separator to hinder current flow (Figure 4c). During cooling with the separator in the anode-facing orientation, we expect the separator to aid current flow (Figure 4d). For these tests, the baseline thermal response for comparison was gathered from a PEC with an unpoled PVDF-BT separator. Experiments were conducted at 120 mV for a heating cycle from 20-50-20 °C and the resulting current was measured (Figure 4e-f). In this case, the current values are reported as an additive deviation (*i.e.*, Δi) from the resting current rather than a current ratio because the resting current for cells containing unpoled or poled PVDF-BT separators is similar.

Figure 4e shows the experimental response of the PEC. Curves are shown for both anode- and cathode-facing orientations and for the cell with the unpoled PVDF-BT separator, labeled as the thermal response. As expected, in the cathode-facing orientation, the measured current increase exceeds the thermal response (an increase of 14.6 μA compared to 10 μA for the thermal response). In the anode-facing orientation, the measured current increase is less than the thermal response (an increase of 4.2 μA compared to 10 μA). Note that during these tests, the

pyroelectric-induced electric field across the separator increases from an initial value of zero to its maximum (or minimum, depending on orientation) value at 50 °C and reduces back to zero on the return path to 20 °C. This behavior is consistent with Equation 2. The electric field does not change direction when the cell shifts from heating to cooling, but simply decreases back to zero.

To confirm that the behavior shown in Figure 4e is not an experimental artifact, we performed simulations of the same test (Figure 4f). Similar to the experimental results, during heating, the PEC in the cathode-facing orientation drew more current than the thermal response. In the anode-facing orientation, the PEC drew less current than the thermal response. Although the effect in the simulation is a little larger in magnitude than in the experimental results, the ratio of change is about the same with the cathode-facing orientation requiring about 40% more current than the thermal response and the anode-facing orientation requiring about half the extra current to maintain the same voltage. Differences in magnitude between experimental and simulated current values are attributed to thermal and electrochemical losses not accounted for in the idealized simulations.

If the PEC is first cooled from its resting state and then heated back up to its resting state, we expect the induced electric field to be in the opposite direction compared to the case in which it is first heated from a resting state (see Figure 4a,c). Additionally, the impedance of the electrode – double layer – electrolyte will increase. Thus, we expect a reduced current flow for the base thermal response (*i.e.*, unpoled PVDF-BT separator). To validate this behavior, we ran the same amperometry tests (*i.e.*, at 120 mV) with the cell cooled from 20 °C to 10 °C and then heated back to 20 °C (see **Figure 5**). The experimental results show the expected behavior with thermal response drawing 5.3 μA less current at 10 °C than at resting state, the cathode-facing

separator drawing 6.9 μA less current, and the anode-facing separator drawing only 4.7 μA less current. Furthermore, the simulated results (Figure 5b) match the experimental behavior well.

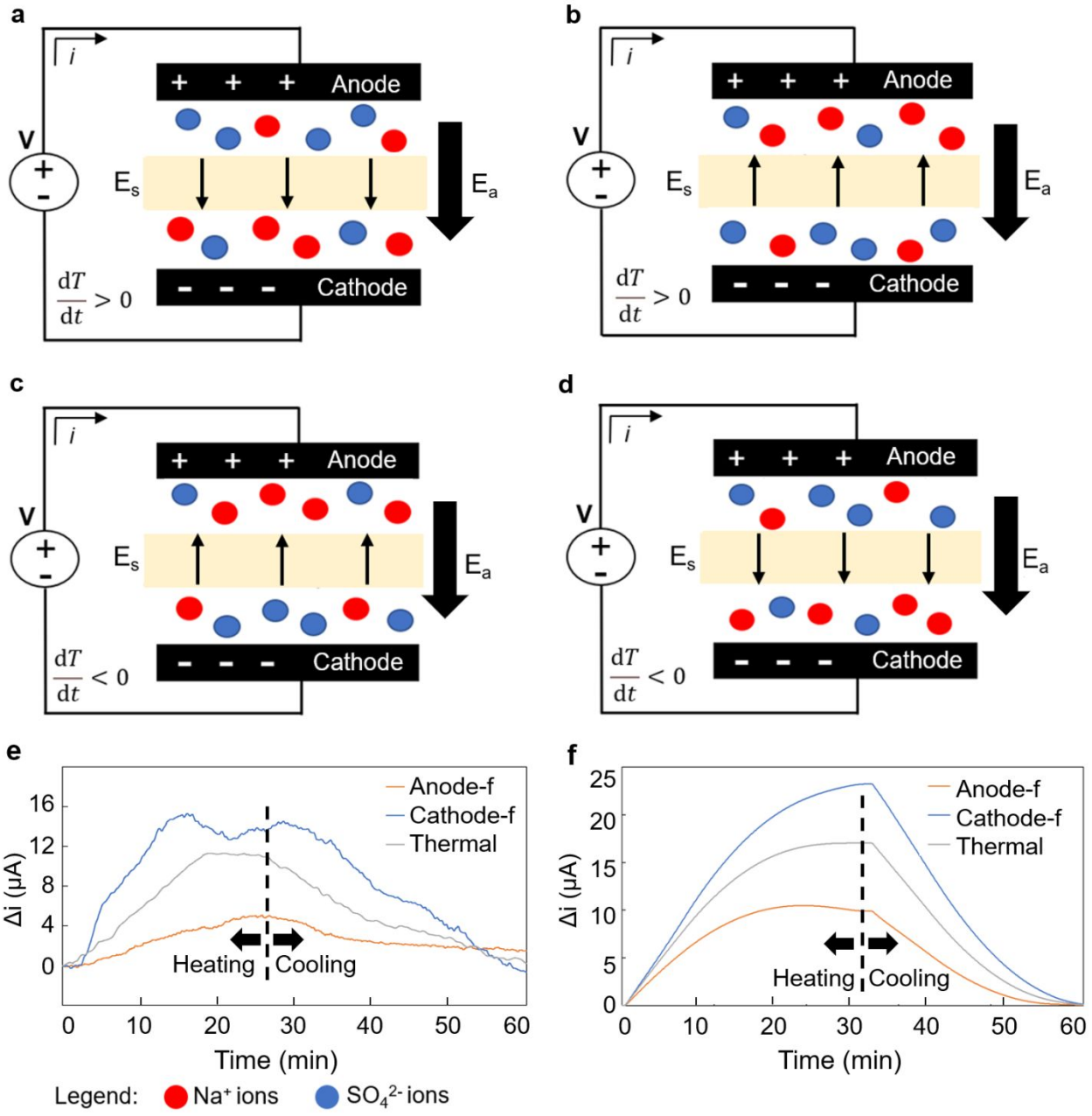

Figure 4. a-d) Schematics of the PEC function during amperometry for the heating and cooling portions of the temperature cycle for both orientations of the PVDF-BT separator, where E_s is the electric field from the separator, and E_a is the field provided by the potentiostat. a) 'Cathode-facing' orientation with heating: the separator will create an electric field driving negative ions towards the anode. b) 'Anode-facing' orientation with heating: negative ions will be driven to the cathode. c) 'Cathode-facing' orientation with cooling: the direction of ion flow is reversed

compared to (a). The separator is driving negative ions towards the cathode. d) 'Anode-facing' orientation with cooling: the separator is now driving negative ions towards the anode. e-f) Experimental (e) and simulated (f) amperometric testing for a 20-50-20 °C thermal cycle for the anode-facing (anode-f) and cathode-facing (cathode-f) separator orientations. The thermal response is that of a non-pyroelectrically active PVDF-BT separator in the PEC.

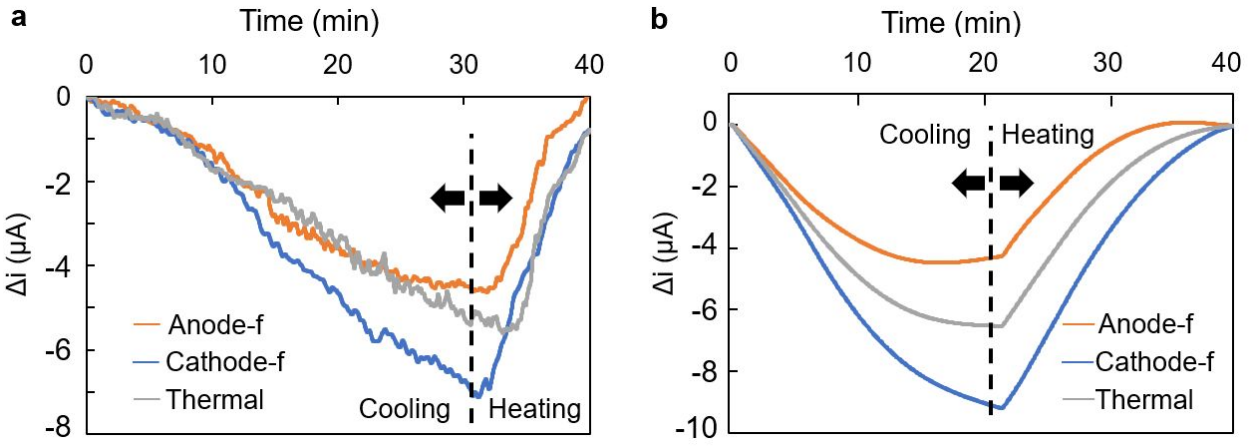

Figure 5. Experimental (a) and simulated (b) amperometric testing for a cooling cycle from 20-10-20 °C of the same PECs as in Figure 4. The effect on amperometric current for each orientation reverses compared to the heating cycle.

To further explore PEC physics during amperometric tests, we simulated the SO_4^{2-} ion concentration at different locations within the cell for the anode-facing, cathode-facing, and thermal separator responses for the 20-50-20 °C thermal cycle. The schematic in **Figure 6** shows the simulated ion concentration profiles from the separator to the anode during heating from 20 °C to 50 °C and cooling back to 20 °C. During the heating phase, ions move away from the separator and into the electrolyte and double layer regions. Within the electrolyte and double layer, we observe an increasing concentration with temperature. The anode-facing orientation exhibits a lower SO_4^{2-} concentration and magnitude of change than the thermal response. The cathode-facing orientation exhibits a greater concentration and larger change compared to the thermal response. This behavior is consistent with the theory of operation in which the pyroelectric separator aids (cathode-facing orientation) or hinders (anode-facing orientation) anion flow toward the anode upon heating. At the inner Helmholtz plane, we observe a small change in ion concentration with temperature for all three simulations. This follows from the theory of the inner Helmholtz plane being set mostly by the ions within the cell and not the cell conditions specifically. The amperometric voltage holds this inner layer relatively stable throughout the heating phase. The mean anion concentration from separator to anode is shown by the dashed vertical lines in Figure 6. Note that all orientations exhibit an increase in the mean concentration with increasing temperature. This is consistent with increased current flow at elevated temperatures. The cathode-facing orientation shows a higher mean concentration relative to the anode-facing configuration, indicative of the increased current the PEC draws during the experimental amperometry results of Figure 4e. These results demonstrate the effect of the pyroelectric separator on ion movement during amperometry, where, for a given direction

of applied voltage, the movement of ions is either increased or decreased depending on the separator orientation.

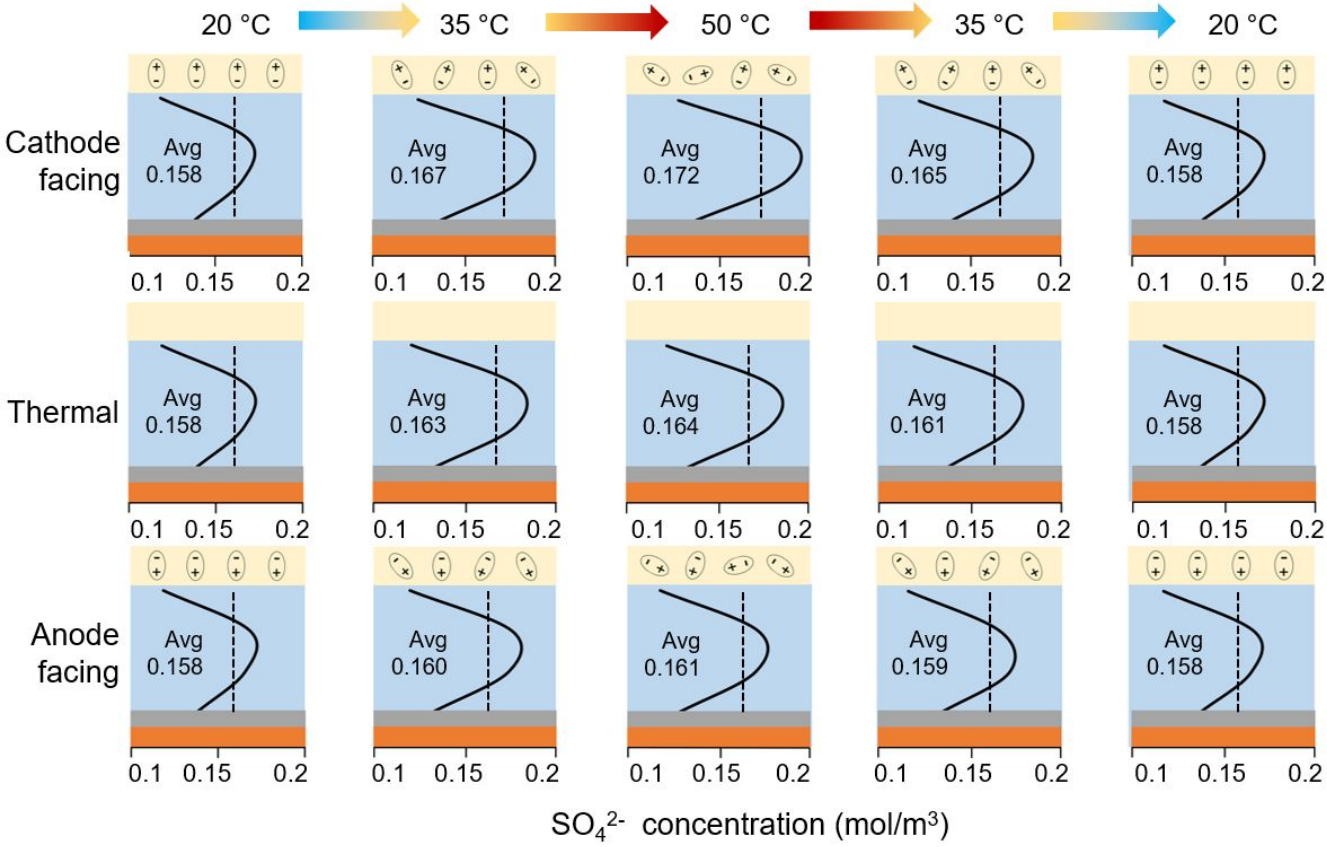

Figure 6. Geometric representation of the change in concentration of SO_4^{2-} ions with temperature during the simulated 20-50-20 °C amperometric testing of Figure 4. Separator orientations are as defined previously. At each temperature the concentration from the separator (top) to the anode surface (bottom) is shown. The average concentration for each state throughout the entire region is shown numerically and as a dashed line. Note that distances are not to scale (see Figure S5 for detailed simulation layout information).

3.3 Variable Temperature Response: Open Circuit Potential

OCP measurements were conducted to investigate the self-charging behavior of the PEC when subject to temperature fluctuations with time. Prior to heating or cooling, the cell is at rest with no pyroelectric field. With heating, the polarization of the separator decreases, inducing an electric field *E* that drives cations from the anode to the cathode, raising the OCP of the cell (**Figure 7a**). With cooling, the opposite effect occurs.

Figure 7b provides experimental and simulation results for PVDF-BT cell OCP with anode- *vs.* cathode-facing separator orientations. The cell was subject to sequential 20-30-20 °C temperature cycles in both experiment and simulation. As shown in Figure 7b experimental results, the cell can be heated or cooled without a rest period between thermal cycles. The extent to which heating or cooling changes the OCP of the pyroelectric cell, and whether this change is positive or negative, depends on the separator orientation with respect to the cell anode or cathode. Differing from the observed phenomena during amperometry, here anode-facing and cathode-facing separator orientations will move the OCP in opposite directions instead of impacting current. Since the cell is symmetric, the direction of the pyroelectric field within the separator will move ions in different directions causing a positive or negative net change in OCP. This result is confirmed through COMSOL simulations, where the only difference between cathode-facing and anode-facing cells is the separator orientation. With both orientations, the OCP of the pyroelectric cell does not return to its at-rest value when the cell returns to its resting temperature. This is due to hysteresis in the structure of the electrochemical double layer arising from heating *vs.* cooling phases of a thermal cycle. Thus, it is possible to continuously increase (or decrease) the OCP with repeated applications of a thermal cycle. COMSOL simulations predict a larger net change in OCP after five thermal cycles than observed experimentally. This

may be due to leakage current in the experimental cell causing self-discharge, which is neglected in the idealized simulation. In the cathode-facing experiment, the OCP stabilized 0.65 mV higher than the at-rest value after four cycles. In the cathode-facing simulation, the OCP increased by 3.3 mV after five cycles (Figure 7b). When the anode-facing orientation is applied, the experimental OCP decreases by -0.5 mV from the at-rest value *vs.* the simulated OCP change of -3.5 mV. Simulation and experimental results both show a decreasing net cycle-to-cycle change in OCP with each successive thermal cycle (cathode-facing and anode-facing orientation). We propose that this is due to capacitive nature of charging the electrochemical double layer. While the pyroelectric field remains constant for each thermal cycle, additional energy is needed to populate the double layer as the cell potential increases (Equation 4).

The OCP of a non-pyroelectric cell also fluctuates with heating and cooling, primarily due to changes in ESR and double layer capacitance with temperature. However, the cell returns to near its at-rest potential at the completion of a thermal cycle (assuming no irreversible changes to the cell have occurred). COMSOL simulations of a Celgard 3501 cell confirm this expected result (Figure 7c). Over five simulated 20-30-20 ^{o}C temperature cycles, the OCP of the Celgard cell fluctuates with temperature, however there is a net 0 mV change in potential over each thermal cycle. While the experimental Celgard cell does not perfectly return to 0 mV as in the simulation, this is expected due to small (mV) fluctuations in OCP that occur over time with real cells, as well as charge redistribution effects that arise from thermal cycling.

COMSOL simulations were used to explore the effect of heating and cooling rate on PEC self-charging. The pyroelectric field and total energy generated by the separator is proportional to dT, as described by Equation 2. If the PEC is subject to thermal cycles with the same T_1 -T_2-T_1 end points but varying dT/dt, we expect differences in cell OCP *vs.* time but the same net ΔOCP.

Simulation results in Figure 7d partially confirm this prediction, with minor differences in ΔOCP observed between the tests. PVDF-BT cells were simulated over a 20-30-20 ^{o}C thermal cycle at 1x, 2x, and 0.5x the *dT/dt* rate presented in Figure 7b. These rates correspond to a peak ΔOCP of 6.11 mV, 6.22 mV, and 6.02 mV, respectively. Post-cycling, the 2x rate returned to a slightly greater OCP than the 1x rate, which returned to a greater OCP than the 0.5x rate. The difference in peak and post-cycling cell OCP with increasing *dT/dt* is likely due to the electric field requirements of charging the electrochemical double layer. With greater *dT/dt*, and subsequently greater pyroelectric field, electrolyte ions are subject to a greater electromotive force that can overcome Coulombic repulsions, effectively filling the double layer with more densely packed ions and resulting in a greater cell voltage. Supporting Information **Figure S7** provides a comparison of two experimental single-cycle OCP tests at heating rates corresponding to 1x *dT/dt* and 2x *dT/dt* rates in Figure 7d. The experiment results show similar net ΔOCP for the two heating rates, supporting our theory of operation.

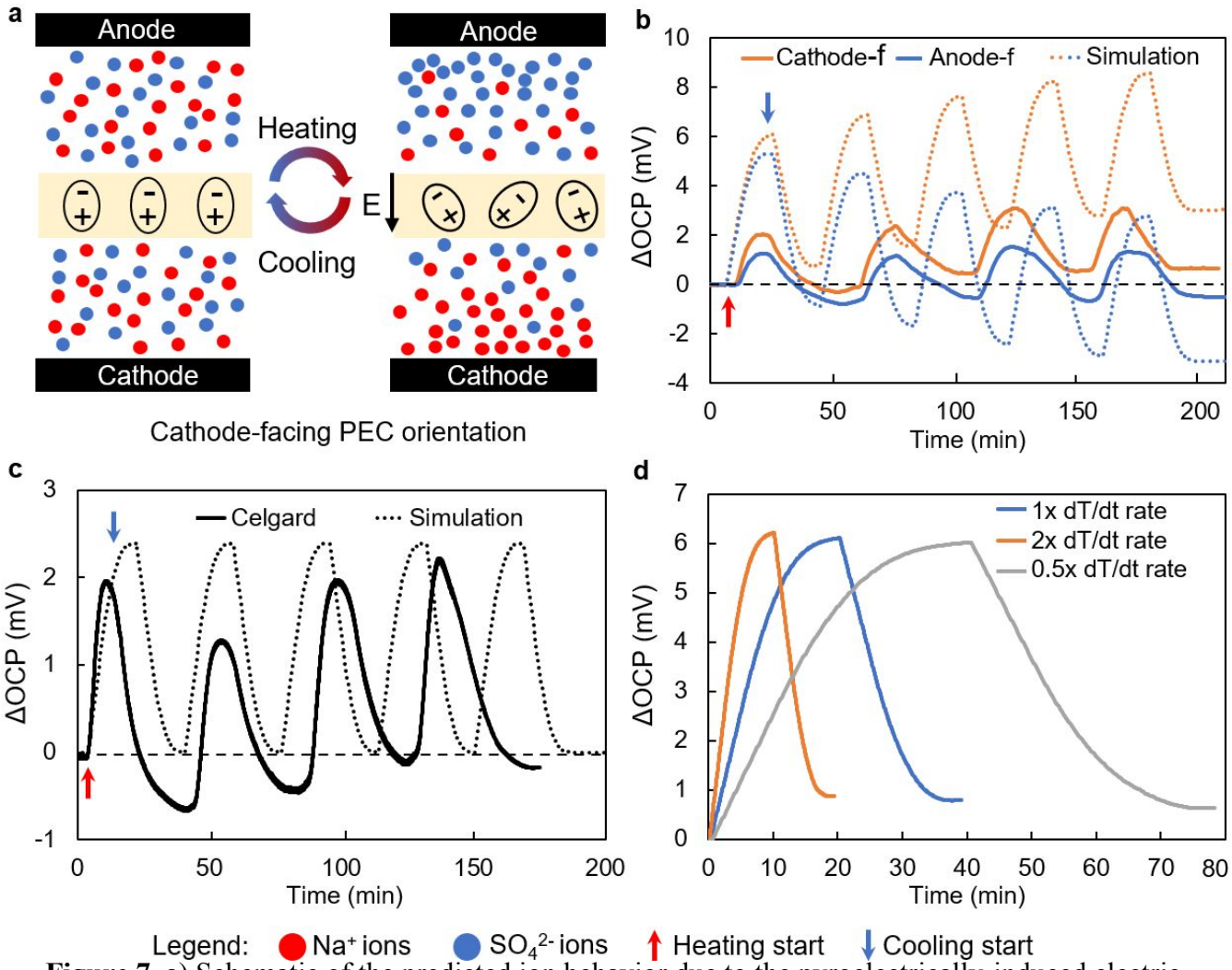

Figure 7. a) Schematic of the predicted ion behavior due to the pyroelectrically-induced electric field in OCP conditions. b) Experimental and simulated changes in OCP for both orientations of the separator over the heating cycles. c) For comparison, the symmetric response of the non-pyroactive Celgard cell under the heating cycles, with no prolonged change in cell OCP seen upon returning to rest state. d) Simulated response of single-cycle OCP testing at different heating rates. The reported 20-30-20 °C heating rate is defined as the 1x rate, with 2x and 0.5x this rate simulated for comparison.

3.4 Outlook and Applications

The PEC is well-suited to IoT applications where consistent thermal cycling is present, including transportation and smart agriculture. Significant *dT/dt* gradients are experienced by, *e.g.*: an airplane cargo hold during transport ($\Delta T \sim 50$ °C);[25] metallic built environment structures exposed to direct sunlight (*e.g.* playground equipment, $\Delta T \sim 70$ °C);[26] and vehicle exhaust components from start-up to operation ($\Delta T \sim 190$-790 °C).[27] In a typical IoT system, approximately 50 to 500 μJ per thermal cycle will enable a single measurement and data transmission event.[28-31] For a broadly applicable benchmark, we use 100 μJ/cm^2 as a "useful" amount of energy for low-power IoT purposes.

To estimate the utility of the PEC, we calculated theoretical energy density (μJ/cm^2) per thermal cycle as a function of ΔT for various pyroelectric separator materials and compared the results with IoT energy requirements and experimental measurements obtained in this work. Theoretical energy density per unit area (U/A) generated by the pyroelectric element and stored in the PEC is calculated using Equation 5, derived from Equation 2 and the relationship for the energy stored in a capacitor:

$$\frac{U}{A} = \eta\left(\frac{h(\rho\Delta T)^2}{2\varepsilon}\right) \quad (5)$$

where ρ, ε, and h are the pyroelectric coefficient, dielectric constant, and thickness of the separator, respectively. The coefficient η represents the conversion efficiency of pyroelectric energy to stored electrochemical energy in the PEC. **Figure 8** plots Equation 5 for two pyroelectric materials (lead zirconate titanate, PZT, and PVDF-BT) and several values of conversion efficiency. Average single-cycle energy values obtained during experimental OCP heating cycles were 2.51 μJ/cm^2 for the 20-30-20 °C cycle and 12.3 μJ/cm^2 for the 20-50-20 °C cycle (calculated using Equation 4). These values, plotted as data points in Figure 8, correspond

to an η value of 17% for the PVDF-BT separator. Single-cycle energy values for COMSOL simulation OCP results, also plotted in Figure 8, correspond to an η value of 37%. Both COMSOL simulation and experimental data points align well with the Equation 5 model. The shaded region in Figure 8 represents the optimization potential of PEC. With improvements in conversion efficiency, pyroelectric material selection, and expanded ΔT range of operation, the PEC is capable of meeting and/or surpassing the IoT target.

Supporting Information **Table S3** compares PEC energy harvesting and storage results achieved in this work with other self-charging power cells reported to-date. Even at the current performance, the average power harvested from the PEC is comparable to that of other self-charging devices. Supporting Information **Table S4** provides comparison with other thermal energy harvesting techniques for added context. Supercapacitor self-discharge through leakage current is a well-known phenomenon with a significant temperature dependence. A preliminary analysis of the expected effects of leakage current on PEC devices is discussed in the Supporting Information. The results provide confidence in the PEC's ability to achieve a net charge with thermal cycling in the presence of leakage current. With future iterations of PEC materials and refined cell construction, it is expected that workable environmental temperature ranges for PEC integration in IoT systems quickly become viable. Furthermore, as the PEC can be charged in heating or cooling mode depending on the separator orientation, there are opportunities to reduce leakage current through self-charging applications at reduced temperatures.

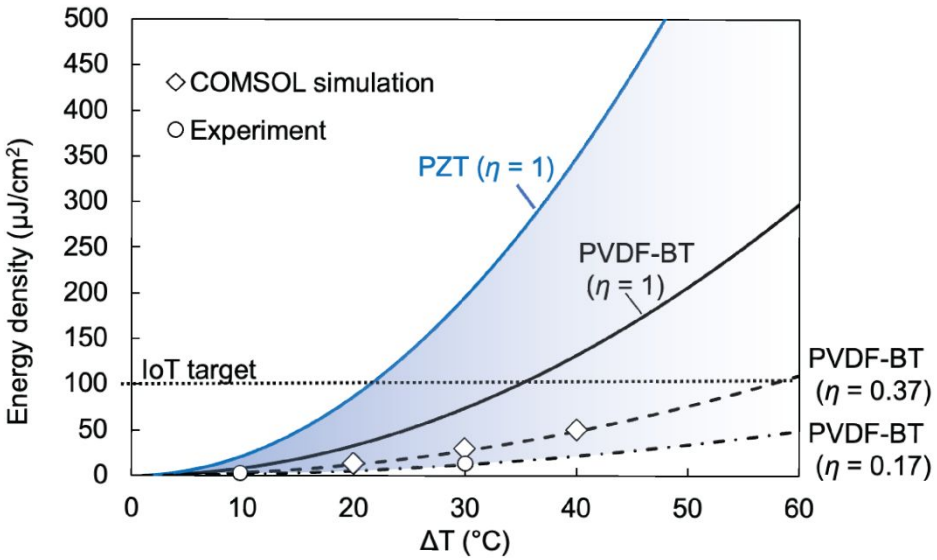

Figure 8. Single-cycle energy density of the PEC plotted as a function of temperature change. Experimentally measured and simulated PEC energy densities (circle and diamond points, respectively) are shown alongside theoretical energy density values calculated using Equation 5. The shaded blue region of the plot represents the optimization potential of the PEC, as compared to a 100 μJ/cm^2 IoT target.

Conclusion

The PEC is a novel device concept for the direct conversion of thermal energy to stored electrochemical energy. PEC theory-of-operation is based on a change in polarization of the pyroelectric separator producing an electric field internal to the cell which drives ion movement across the cell. Experimental and simulation results validate the expected change in PEC current or voltage response depending on the magnitude and direction of dT/dt, and the orientation of the pyroelectric separator relative to the cell anode and cathode. Based on an analysis of application targets and thermal energy availability, we propose that an optimized and well-constructed PEC has the potential to harvest enough energy to supply IoT devices with 100 $\mu J/cm^2$. This energy could be harvested and stored each thermal cycle in circumstances where ΔT is < 60 °C, safely below the device limit and a low enough thermal change to make application areas abundant.

Declaration of Competing Interest

The authors declare that they have no known competing financial interests or personal relationships that could have appeared to influence the work reported in this paper.

Acknowledgments

This work is supported by the National Science Foundation (Award No. 1936636).

Supporting Information

PEC design

Temperature profiles applied during experimentation and simulation

Experimental reproducibility

Separator orientation methods

COMSOL Multiphysics simulation

PVDF-BT and Celgard pyroelectric response

PVDF-BT vs. Celgard cell EIS and CV comparison

Experimental single cycle heating rate comparison

Self-charging power cell performance comparison

Thermal energy harvester performance

Leakage current assessment

References:

[1] Z. Wang, X. Liu, M. Yue, H. Yao, H. Tian, X. Sun, Y. Wu, Z. Huang, D. Ba, Hybridized energy harvesting device based on high-performance triboelectric nanogenerator for smart agriculture applications. Nano Energy 2022, 102, 107681.

[2] A. Aabid, M. A. Raheman, Y. E. Ibrahim, A. Anjum, M. Hrairi, B. Parveez, N. Parveen, J. M. Zayan, A systematic review of piezoelectric materials and energy harvesters for industrial applications. Sensors 2021, 21, s21124145.

[3] J. Wang, T. He, C. Lee, Development of neural interfaces and energy harvesters towards self-powered implantable systems for healthcare monitoring and rehabilitation purposes. Nano Energy 2019, 65, 104039.

[4] X. Wang, Z. Ning, X. Hu, L. Wang, L. Guo, B. Hu, X. Wu, Future communications and energy management in the internet of vehicles: toward intelligent energy-harvesting. IEEE Wire. Comm. 2019, 26, 1900009.

[5] X. Xue, S. Wang, W. Guo, Y. Zhang, Z. L. Wang, Hybridizing energy conversion and storage in a mechanical-to-electrochemical process for self-charging power cell. Nano Lett. 2012, 12, nl302879t.

[6] A. Ramadoss, B. Saravanakumar, S. W. Lee, Y. Kim, S. J. Kim, Z. L. Wang, Piezoelectric-driven self-charging supercapacitor power cell. ACS Nano 2015, 9, 5b00759.

[7] H. He, Y. Fu, T. Zhao, X. Gao, L. Xing, Y. Zhang, X. Xue, All-solid-state flexible self-charging power cell basing on piezo-electrolyte for harvesting/storing body-motion energy and powering wearable electronics. Nano Energy 2017, 39, 2017.07.033.

[8] S. Roy, P. Thakur, N. A. Hoque, A. Kool, F. Khatun, P. Biswas, B. Bagchi, S. Des, Self-charging photo-power cell based on a novel polyer nanocomposite film with high energy density and durability. Poly. J. 2019, 51, s41428.

[9] A. Maitra, S. Paria, S. K. Karan, R. Bera, A. Bera, A. K. Das, S. K. Si, L. Halder, A. De, B. B. Khatua, Triboelectric nanogenerator driven self-charging and self-healing flexible asymmetric supercapacitor power cell for direct power generation. ACS Appl. Mater. Inter. 2019, 11, 8b19044.

[10] X. Shi, S. Chen, H. Zhang, J. Jiang, Z. Ma, S. Gong, Portable self-charging power system via integration of a flexible paper-based triboelectric nanogenerator and supercapacitor. ACS Sust. Chem. Eng. 2019, 7, 9b05129.

[11] B. Yu, J. Duan, J. Li, W. Xie, H. Jin, R. Liu, H. Wang, L. Huang, B. Hu, J. Zhou, All-day thermogalvanic cells for environmental thermal energy harvesting. Research 2019, 2460953.

[12] Y. Yang, S. Lee, H. Ghasemi, G. Chen, Charging-free electrochemical system for harvesting low-grade thermal energy. Appl. Phys. Sci. 2014, 111, 1415097111.

[13] T. Kowalchik, F. Khan, K. Le, P. Leland, S. Roundy., R. Warren, Effect of pore structure on the piezoelectric properties of barium titanate-polyvinylidene fluoride composite films. Nano Energy 2023, 109, 108276.

[14] J. Kim, Z. Wu, A. Morrow, A. Yethiraj, Self-diffusion and viscosity in electrolyte solutions. J. Phys. Chem. B. 2012, 116, 306847.

[15] L. Xu, Y. Pang, D. Huang, H. Zhuang, W. Liu, T. Luo, P. H. Lee, L. Feng, J. Lu, The role of sodium sulfate supporting electrolyte in ammonium transport and reduction at interface between platinum cathode and solution. ChemRxiv 2019, 10006712.

[16] J. Mollerup, M. Breil, Modeling the permittivity of electrolyte solutions. AlChE J. 2015, 61, 14799.

[17] D. Luong, M. Sephton, J. Watson, Subcritical water extraction of organic matter from sedimentary rocks. Analy. Chim. Acta 2015, 879, 2015.04.027.

[18] T. Kowalchik, F. Khan, S. Roundy, R. Warren, Direct thermal-to-electrochemical energy conversion via a pyroelectrochemical cell. in 21st Int. Conf. Micro Nanotech. Power Gen. Energy Conv. Appl. (PowerMEMS), IEEE, Utah 2022.

[19] H. Gualous, D. Bouquain, A. Berthon, J. Kauffmann, Experimental study of supercapacitor serial resistance and capacitance variations with temperature. J. Power Sources 2003, 123, 775300527.

[20] V. Potoskaya, O. Gichan, On the origin of phase angle in Warburg finite length diffusion impedance. Int. J. Electrochem. Sci. 2019, 14, 2019.08.97

[21] M. Haque, Q. Li, C. Rigato, A. Rajaras, A. D. Smith, P. Lundgren, P. Enoksson, Identification of self-discharge mechanisms of ionic liquid electrolyte based supercapacitor under high-temperature operation. J. Power Sources 2021, 485, 229328.

[22] N. Yao, L. Yu, Z. Fu, X. Shen, T. Z. Hou, X. Liu, Y. C. Gao, R. Zhang, C. Zhao, X. Chen, Q. Zhang, Probing the origin of viscosity of liquid electrolytes for lithium batteries. Angewandte Chemie, 2023, e202305331.

[23] A. Barua, A. Paul, Unravelling the role of temperature in a redox supercapacitor composed of multifarious nanoporous carbon@hydroquinone. RSC Adv. 2020, 10, c9ra09768f.

[24] G. Xiong, A. Kundu, T. Fisher, Influence of Temperature on Supercapacitor Performance. In: Thermal Effects in Supercapacitors, Springer, Cham 2015, Ch 4.

[25] W. Pelletier, K. V. Chau, R. A. Bucklin, J. K. Brecht, D. W. Hahn, J. Émond, Analysis of air cargo temperature variations during transport operations. Trans. ASABE 2018, 61, 12524.

[26] S. Pfautsch, A. Wujeska-Klause, J. Walters, Outdoor playgrounds and climate change: importance of surface materials and shade to extend play time and prevent burn injuries. Build. Environ. 2022, 223, 109500.

[27] P. Bencs, M. Alktranee, The potential of vehicle cooling systems. J. Phys. Conf. Ser. 2021, 1935, 012012.

[28] T. Bouguera, J. F. Diouris, J. J. Chaillout, R. Jaouadi, G. Andrieux, Energy consumption model for sensor nodes based on LoRa and LoRaWAN. Sensors 2018, 18, s18072104.

[29] M. Germer, U. Marshncer, A. Richter, Energy harvesting for tire pressure monitoring systems from a mechanical energy point of view. IEEE Internet Things J. 2022, 9, 3152547.

[30] C.Bowen, M. Arafa, Energy harvesting technologies for tire pressure monitoring systems. Adv. Energy Mat. 2015, 5, 201401787.

[31] Y. Zhang, F. Zhang, Y. Shakhsheer, J. Silver, A. Klinefelter, M. Nagaraju, J. Boley, J. Pandey, A. Shrivastava, E. J. Carlson, A. Wood, B. H. Calhoun, B. P. Otis, A batteryless 19μW MICS/ISM-band energy harvesting body area sensor node SoC. In IEEE Int. Solid-state Circuits Conf., IEEE, California 2012.